CONCRETE LIBRARY OF JSCE NO. 38, DECEMBER 2001

EXPERIMENTAL STUDY OF LOCALIZATION PARAMETERS IN CONCRETE SUBJECTED TO COMPRESSION

(From Proceedings of JSCE, No.669/V-50, February 2001)


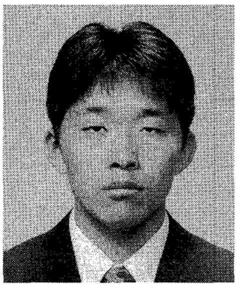
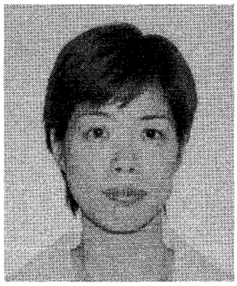
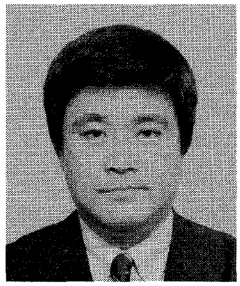

Torsak LERTSRISAKULRAT Ken WATANABE Maki MATSUO Junichiro NIWA

An experimental program involving the measurement of the local vertical strain distribution within a concrete specimen has been conducted to examine the failure mechanism and localization effect of concrete under uniaxial compression. This leads to a new quantitative approach to localized compressive fracture length. By considering the geometrical parameters and properties of the concrete used, it is found that, when localization occurs, the localized compressive fracture length depends only on the size of the cross-section of the specimen. A new definition of fracture energy under compression in terms of externally applied energy per unit fracture volume is also introduced.

Key Words: *fracture mechanics, localization, size effects, fracture energy in compression, localized compressive fracture length*

Torsak Lertsrisakulrat is a doctoral student in the Department of Civil Engineering at Tokyo Institute of Technology. His research interests include problems regarding localized compressive failure of concrete under compression. He is a member of JSCE and JCI.

Ken Watanabe is a master student in the Department of Civil Engineering at Tokyo Institute of Technology. His research interests concern the experimental method to capture the compressive localized failure phenomenon of concrete. He is a member of JSCE and JCI.

Maki Matsuo is research associate in the Department of Civil Engineering at Tokyo Institute of Technology. Her research interests include problems regarding localization analysis of reinforced concrete structures. She is a member of JSCE and JCI.

Junichiro Niwa is a Professor in the Department of Civil Engineering at Tokyo Institute of Technology. He received his Doctor of Engineering degree from the University of Tokyo. He specializes in the mechanics of concrete structures including fracture mechanics and nonlinear numerical analysis. He is a member of JSCE, JCI, IABSE, fib and ACI.

1. INTRODUCTION

It is now generally accepted that the failure of concrete in tension is localized within a limited zone. Many researchers have studied the localization behavior of concrete in tension, and useful results have been obtained[1]. The localized behavior in tension is generally modeled by a stress-crack width relationship based on the tensile fracture energy (G_F). A uniaxial description of the properties is sufficiently realistic, because no major lateral deformations take place simultaneously.

On the other hand, material models for compressive failure of concrete are normally based on a uniaxial compressive stress-strain curve obtained from tests, where uniform deformation throughout the concrete specimen is assumed. This assumption is reasonable for the ascending branch of the stress-strain curve, but is not necessarily accurate for the descending branch. Since it has been found that deformation after the peak stress is localized within certain zones[2], the descending branch of the stress-strain curve becomes size dependent as the measured strain depends on the gage length and position of the gage[3].

Despite a number of studies[4],[5], the localization behavior and fracture zone of concrete in compression have not yet been clarified. Compressive failure is more complex than tensile failure, because it is always accompanied by significant lateral deformations. These lateral deformations are mainly caused by splitting cracks, which form and expand during the failure process. In addition to these cracks, localized shear bands may also form. Thus, the fracture process in compression is not only determined by localized cracks, as in tension; rather to be realistic, both the local and the continuum components of compressive softening have to be taken into account.

In order to analyze the post-peak behavior of concrete in a more realistic manner, it is necessary to study the behavior of concrete under compression in consideration of crack localization and fracture energy of concrete in compression. Furthermore, a realistic stress-strain curve for concrete under uniaxial compression that takes into account localization behavior will lead to more accurate results in the analysis of bending stresses in reinforced concrete members[6].

2. REVIEW OF PREVIOUS RESEARCH

The problem of accurately determining localized compressive length has often been discussed. Markeset and Hillerborg[5],[7] took the value of damaged zone, L^d, to be 2.5 times the smallest lateral dimension of the concrete cross-section. This proposed value was based on the finding of other researchers[3],[8] that the compressive strength, f_c', of a specimen becomes constant when the slenderness ratio reaches a value of about 2.5. This constant value of f_c' is obtained regardless of the test technique and end restraint conditions. However, there has been no direct measurement of the fracture length for the suggested value of L^d.

In 1999, an attempt to measure the localized compressive fracture length was made by Nakamura and Higai[4]. They obtained the localized compressive fracture length by considering the local strain, as measured by embedding a deformed acrylic bar fitted with strain gages within concrete cylinder specimens. It was found that the localization behavior could be captured effectively, but no clear evaluation method of localized compressive fracture length was presented and the parameters of the study mainly focused on properties of the concrete used to cast the specimens.

On the other hand, the definition of fracture energy in compression also remains uncertain. Nakamura and Higai[4] defined the local fracture energy, G_{fc}, as the energy absorbed per unit area in the fracture zone. This was estimated from the area under the overall load-deformation curve excluding the elastic unloading part. The compressive fracture energy, W_q, was alternatively defined as the energy dissipated up to the point where the load descends to 1/3 of the peak load; this includes a portion of the elastic strain energy as presented by Rokugo and Koyanagi[9].

In this investigation, an experimental program is conducted in order to clarify the localized behavior of concrete in compression. The experiment is divided into two parts. The first considers the wide range of geometrical parameters such as the height-depth ratio, shape and size of a specimen. The effects of these parameters on localized compressive fracture length and fracture energy in compression of concrete under uniaxial compressive stress are determined while holding properties of the concrete constant.

The effects of concrete properties (i.e. cylindrical compressive strength and maximum size of coarse aggregate) on localized compressive fracture length and fracture energy in compression are subsequently examined in the second part of the experiment. In all tests, high early strength cement is used. Finally, a quantitative judgment of localized compressive fracture length and a definition of compressive fracture energy are introduced.

3. EXPERIMENT

3.1 Part I

The effects of the geometrical parameters height-depth ratio, size and shape of the specimen on failure relating to localized compressive fracture length and compressive fracture energy were examined. Details of the experimental program are listed in Table 1(a).

All specimens were cast using concrete with the same mix proportion and an average cylindrical compressive strength of 45 N/mm^2. The quantities of materials used are shown in Table 1 (b). The tops of specimens were capped with cement paste 6-8 hours after casting to ensure a smooth horizontal surface for loading. Specimens were demolded after one day and cured in water at about 22 °C for 7 to 8 days before testing. Compressive strength tests were also carried out on concrete cylinders ϕ 100 × 200 mm taken from the same concrete batch.

The technique of measuring strain within a concrete specimen by embedding a deformed acrylic resin bar, as studied by Nakamura and Higai[4], was found to be effective and was adopted in this experiment. The square-section acrylic resin bar with a cross-section of 10 × 10 mm was first deformed by cutting half cylinder-shaped furrows across the two opposite faces in order to ensure good bonding between the bar and concrete, as shown in Fig.1 (a). Strain gages were attached to the bar which was then installed vertically in a position coincident with the specimen axis before casting of the concrete. The strain gages were attached in a vertical orientation to measure the longitudinal local strain at intervals of 40 mm (or 20 mm in the case of 100 mm height specimens). The total deformation of a specimen was externally measured during loading by the use of deflection gages set between the loading plates. Friction at the interfaces between the ends of a concrete specimen and the loading platens was reduced by inserting friction-reducing pad sets consisting of two teflon sheets sandwiching silicon grease. In the case of the standard cylindrical compressive strength tests on the ϕ 100 × 200 mm cylinder, no attempt was made to reduce friction between specimen ends and the loading plates. The installation of the deformed acrylic bar and the test arrangement are also illustrated in Fig.1. All data were recorded using a data logger.

Post-peak load-deformation curves were captured by one-directional repeated loading in the stress descending range. The initiation and propagation of cracks were also visually observed.

Table 1 Experimental Program: Part I

(a) Experimental program

Specimen	Cross-section (mm × mm)	Height (mm)	H/D	Designation
Prism	200 × 200	800	4	PS20-80
		400	2	PS20-40
		200	1	PS20-20
	200 × 100	800	4	PR20-80
		400	2	PR20-40
		200	1	PR20-20
	100 × 100	400	4	PS10-40
		200	2	PS10-20
		100	1	PS10-10
Cylinder	ϕ 200	800	4	C20-80
		400	2	C20-40
		200	1	C20-20
	ϕ 100	400	4	C10-40
		200	2	C10-20
		100	1	C10-10

**Average cylindrical compressive strength at 7 days for all cases is 45 N/mm^2 with the maximum size of coarse aggregate 20 mm.*

(b) Mix proportion of concrete**

Name of mixture	G_{max} (mm)	W/C (%)	s/a (%)	Weight per unit volume (kg/m^3) W	C	S	G (mm) 5-13	13-20
25	20	50	45	185	370	799	494	494

***No admixture; air content is 2.0%.*

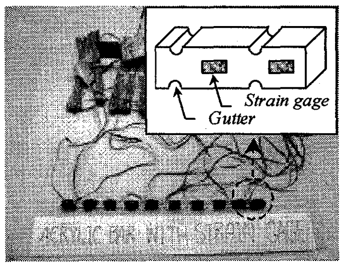

(a) Acrylic bar with strain gages

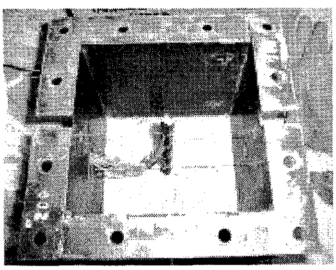

(b) Installation of acrylic bar

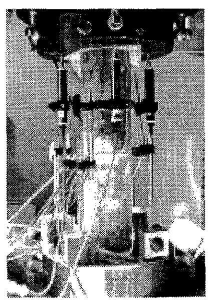

(c) Loading set up

Fig.1 Installation of strain gages and test arrangement

3.2 Part II

In this part of the experiment, only cylinder specimens ϕ 100×400 mm were used in the testing program. Once again, a deformed acrylic bar fitted with strain gages was embedded inside all specimens. The concrete properties, i.e. maximum size of coarse aggregate, G_{max}, and water-cement ratio, W/C, were varied as shown in Table 2. The specimen preparation process was the same as in Part I, except that instead of capping the tops of specimens, the tops of the specimens were ground.

The testing procedures were also the same as in Part I.

Table 2 Experimental program: Part II*

Name of mixture	G_{max} (mm)	W/C (%)	s/a (%)	Weight per unit volume (kg/m^3)				
				W	C	S	G (mm) 5-13	G (mm) 13-20
15		50	49	190	380	853	898	-
16	13	60	51	190	317	915	889	-
17		70	53	190	271	970	870	-
25		50	45	185	370	799	494	494
26	20	60	47	185	308	859	490	490
27		70	49	185	264	913	481	481

*No admixture was added and the air content for G_{max} 13 and 20 mm is 2.5% and 2.0%, respectively.

4. DETERMINATION OF LOCALIZED COMPRESSIVE FRACTURE LENGTH AND FRACTURE ENERGY IN COMPRESSION

After compiling all test results, the overall average stress-strain curves from external measurements, together with the local stress-strain curves measured by each gage attached to the deformed acrylic bar, were plotted. As an example, the PS10 series of specimens are shown in Fig.2 (a) and (b). Here, σ_{max} and ε_0 refer to the maximum stress and corresponding strain, respectively.

4.1 Localized compressive fracture length, L_p

It can be seen from the local stress-strain curves of PS10-40 shown as in Fig.2 (b) (full results including the numerical values for PS10-40 are summarized in APPENDIX A) that, in the stress descending range, some parts of the specimen exhibit softening behavior (increasing strain) while others show unloading behavior (decreasing strain). Thus, in this case, failure was localized into a certain part of the specimen.

As cited before, many attempts have been made to set up the value of fracture length or localized compressive fracture length, L_p, on the basis of test results. Most did not directly measure the value of L_p, but rather theoretically derived it[6], or else based it on the part of the specimen believed to be subjected to uniform uniaxial compressive stress[5),7)]. One attempt to directly measure L_p was made by Nakamura and Higai[4)],but the determination of L_p in their study was based on the ability to distinguish between the zone of increasing local strain (the softening zone) and the zone of decreasing strain (the unloading zone), which is somewhat subjective. This problem also became apparent in this study when some parts of a specimen showed unloading behavior at the beginning of the descending path, but then exhibited softening behavior when the load was further increased, as seen in curves for gage numbers 3 to 6 in Fig.2 (b).

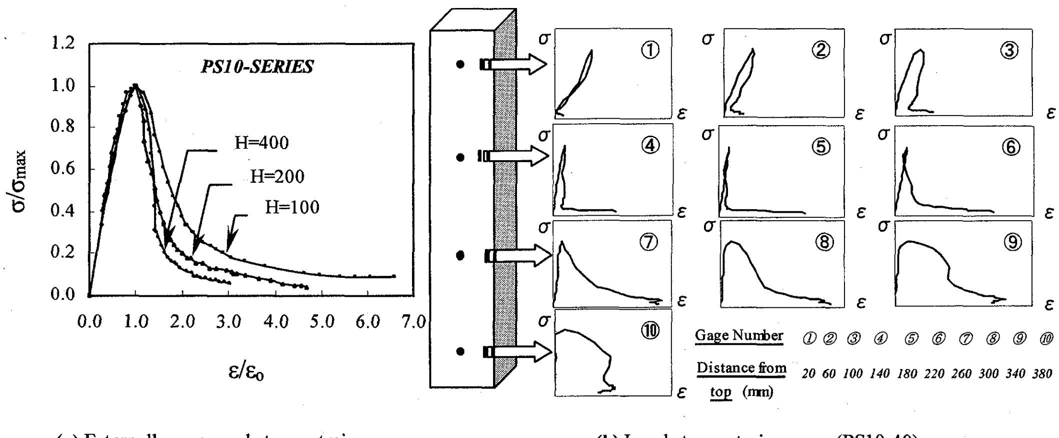

(a) Externally measured stress-strain curves

(b) Local stress-strain curves (PS10-40)

Fig.2 Typical results from experiment Part I (PS10-SERIES)

Given these problems, a newly developed concept for the determination of L_p is introduced in this paper. The energy consumed by each portion of a specimen, as calculated from the load-local deformation curve, is used as the criterion for judgment of L_p.

From the load-local deformation curves of a specimen, the energy absorbed by the whole specimen can be calculated by summing up the energy absorbed in each portion of the specimen, assuming that there is constant strain in the intervals between strain gages, as depicted in Fig.3. Figure 3 (a) shows the portion assumed to have constant strain, while Fig.3 (b) shows the area beneath the descending part of the load-local deformation, P-d_i, curve for that specimen portion until the load falls to 10% of that at the maximum resistance, P_{max}. The calculated area, i.e. the shaded area, therefore, is the energy consumed within that portion of the specimen; this will be called $A_{int\,i}$. The summation of $A_{int\,i}$ over the whole specimen yields the total energy consumed, or A_{int}, as shown in Eq. (1).

$$A_{\text{int}} = \sum_{i=1}^{n} A_{\text{int}\,i} \qquad \text{(N-mm)} \qquad (1)$$

where, n is the total number of gages attached to the deformed acrylic bar.

Therefore, a distinct and objective definition of the compressive fracture zone is then obtained as the zone in which the value of $A_{int\,i}$ is larger than 15 percent of A_{int}, and the length of this zone is called the localized compressive fracture length, L_p (Fig.3 (c)). The 15 percent criterion is selected because calculated values of L_p correlate well with the experimental observations at this level. In addition, for portions in which $A_{int\,i}$ is greater than 15 percent of A_{int}, it can be perceived that the energy absorbed is considerably high and enough to lead to failure.

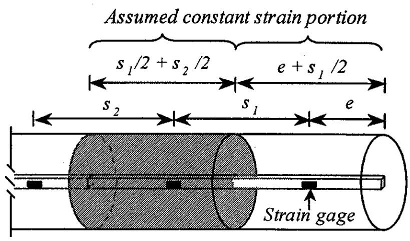

(a) Assumed length of uniform strain distribution

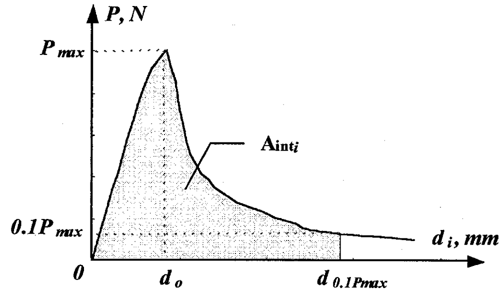

(b) Energy consumed by each portion, $A_{int\,i}$
(Load-local deformation curve)

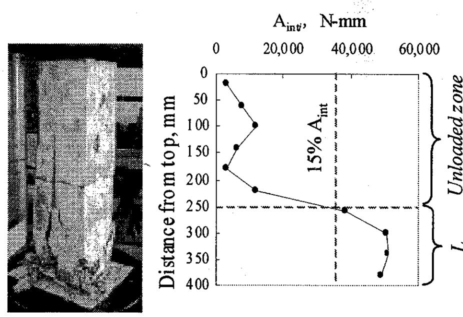

(c) Localized compressive fracture zone

Fig.3 Determination of L_p

4.2 Compressive fracture energy, G_{Fc}

The definition of compressive fracture energy has also been suggested by many researchers. Nakamura and Higai[4] defined the local compressive fracture energy in terms of absorbed energy, as provided by an externally applied load up to 20% of P_{max}, within the softening range excluding the elastic unloading path, per unit area of the specimen cross-section. On the other hand, Rokugo and Koyanagi[9] defined the total absorbed energy up to 1/3 (approximately 33%) of P_{max} in the descending range as the compressive fracture energy. It is clear that a universal definition has yet to be set up. One reason may arise from the lack of reliable data on fracture length, L_p. Hence, in this paper, based on the newly developed criterion for L_p, G_{Fc} is evaluated from the energy consumed by the specimen up to 10% of P_{max} within the descending range and the true fracture volume, V_p, resulting from the externally applied load. This concept of G_{Fc} based on fracture volume, V_p, (not area) is introduced here since, in a realistic interpretation, the externally applied energy would cause a volumetric failure rather than failure at any specific cross-section of a specimen. Further, the value of 10% of P_{max} is chosen because, from the experiments, it was found to be the level of load at which further loading would cause only a small change in total specimen deformation.

Just as for $A_{int\,i}$, A_{ext} can be calculated from the externally measured load-overall deformation, P-d, curve. That is, A_{ext} is the total energy supplied by the external load that causes failure of the specimen. The main place of failure is the localized fracture volume, V_p, which is the product of L_p and the specimen cross-sectional area, A_c. Therefore, the compressive fracture energy, G_{Fc}, or the applied energy per unit volume of the fracture zone, can be calculated by dividing the obtained A_{ext} by V_p, as shown in Eq.(2).

Table 3 Summary of test results

(a) Part I

	Specimen	Section (mm)	A_C (mm^2)	H (mm)	H/D	σ_{max} (N/mm^2)	f_c' (N/mm^2)	σ_{max} / f_c' (%)	L_p (mm)	G_{Fc} (N/mm^2)
PRISM	PS20-80	200×200	40,000	800	4	30.1	47.5	63.3	120	0.694
	PS20-40			400	2	29.7	43.5	68.3	90	0.462
	PS20-20			200	1	23.7	39.6	59.8	160	0.165
	PR20-80	200×100	20,000	800	4*	30.5	39.4	77.2	220	0.530
	PR20-40			400	2*	35.7	43.5	82.1	150	0.238
	PR20-20			200	1*	37.6	50.4	74.6	200	0.176
	PS10-40	100×100	10,000	400	4	30.5	46.7	65.4	145	0.216
	PS10-20			200	2	39.4	50.4	58.2	130	0.182
	PS10-10			100	1	25.7	47.3	54.3	50	0.188
CYLINDER	C20-80	ϕ200	31,416	800	4	34.3	47.5	72.3	130	0.352
	C20-40			400	2	28.1	43.5	64.6	95	0.386
	C20-20			200	1	22.5	50.4	44.6	160	0.150
	C10-40	ϕ100	7,854	400	4	30.5	45.6	66.9	135	0.189
	C10-20			200	2	31.2	39.9	78.1	120	0.206
	C10-10			100	1	20.0	39.6	50.5	100	**

**For PR20-SERIES, D = 200 mm was used.*
*** Result not available.*

(b) Part II

Cross-section × length (mm)	Maximum size of aggregate (mm)	Water-cement ratio	σ_{max} (N/mm^2)	f_c' (N/mm^2)	σ_{max} / f_c' (%)	L_p (mm)	G_{Fc} (N/mm^2)
Cylinder ϕ100×400	*20*	0.50	32.5	45.7	71.1	115	0.215
		0.60	30.4	36.7	82.8	110	0.239
		0.70	22.6	28.4	79.6	148	0.186
	13	0.50	39.4	46.4	84.9	120	0.261
		0.60	29.4	32.2	91.3	118	0.225
		0.70	21.8	26.2	83.3	125	0.178

$$G_{Fc} = \frac{A_{ext}}{V_p} \qquad \text{(N/mm}^2\text{)} \qquad (2)$$

where, V_p = Localized fracture volume, mm^3 $= L_p \times A_c$
A_c = Concrete cross-sectional area, mm^2

The results of L_p and G_{Fc} for Parts I and II of the experiment are summarized in Table 3(a) and (b), respectively.

5. CRACKING PATTERNS

Many researchers have reported the effects of end restraint on the measured stress-strain curve of concrete under uniaxial compression[3), 8), 10)]. Thus, as mentioned above, in all tests here, an attempt was made to reduce friction between specimen ends and the loading platens by inserting friction-reducing pads. From the test results shown in Table 3(a) and (b), the ratios of the maximum specimen stress to cylindrical compressive strength, σ_{max}/f_c', vary. However, the average values are 71% and 76% when H/D=2 and 4, respectively, which means the friction was effectively eliminated by the friction-reducing pads.

In the case of H/D = 1, the average σ_{max}/f_c' is 57%. The reason for this low value is that specimens with H/D=1 failed in splitting failure mode, which is completely different from the cases when H/D≥2.

Moreover, from the observation of cracks, it was found that, for specimens with H/D≥2, failure did not commence at the central zone of a specimen but was initiated from one end, meaning that the effects of end restraint were substantially eliminated. An additional reason arises because of the nature of concrete; it is inhomogeneous and its strength over the specimen length takes the form of a normal distribution. Hence, stable failure throughout the length cannot be expected. Furthermore, certain unavoidable imperfections in the testing arrangement, such as the horizontality of the loading plate, mean that perfectly uniform force transfer from the ends is unlikely to be achieved, especially when the length of the specimen is greater; therefore, the failure is likely to be initiated from one end of the specimen.

5.1 Experiment Part I

From observations of crack occurrence in tested specimens, it can be seen that, for short specimens with H/D=1, failure consisted of splitting from top to bottom of the specimen and the observed value of compressive fracture length, L_p, is, in almost all cases, equal to H. As for the longer specimens with H/D=2 and 4, lots of small visible vertical cracks were observed in a particular region when the peak resistance was reached. At the final stage, in the post-peak region at $0.1P_{max}$, the small cracks coalesced to form the crack zone while a few long vertical cracks penetrated down to the bottom (in a case where the specimen failed from the top). Thus localization occurred only for H/D≥2, and later sections discussing L_p and G_{Fc} will refer to only the results for specimens having H/D≥2. This localization behavior can also be clearly seen in the photographs of the cracking pattern at the final stage shown in Fig.4.

It should be noted that, compared with the work done by Markeset[5], these vertical cracks are assumed to be localized into a shear band but positioned vertically in this experiment, because friction at the ends was effectively removed.

5.2 Experiment Part II

Further observations on the effects of maximum size of coarse aggregate and water-cement ratio on localization in compression were carried out. Concrete cylinder specimens with a diameter of 100 mm and a height of 400 mm were selected and tested. Typical results are depicted in Fig.5.

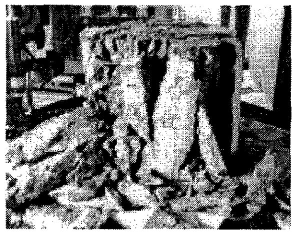

(a) H/D = 1

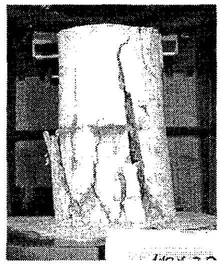

(b) H/D = 2

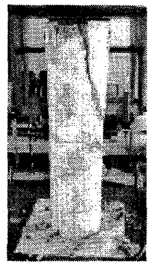

(c) H/D = 4

Fig.4 Cracking patterns of tested specimens (C10-SERIES) (experiment Part I)

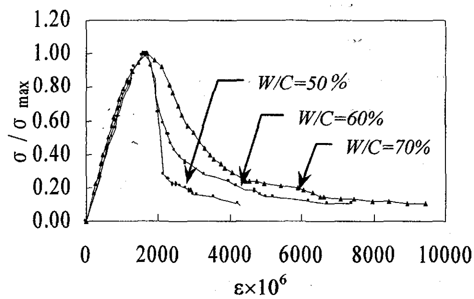

Fig.5 Typical results from experiment Part II (G_{max} = 20 mm)

From the observation of cracks during the tests, examples of which are shown in Fig.6 (a) and (b), it is clear that localization occurred in some parts of specimens with a few penetrating long cracks as in experiment Part I. There is no

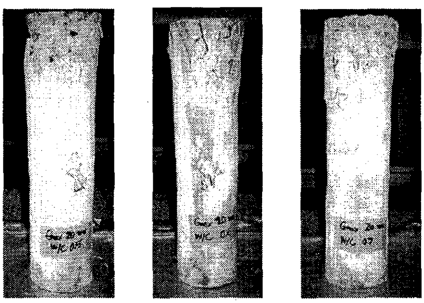

W/C=0.50 *W/C=0.60* *W/C=0.70*

(a) G_{max} = 20 mm

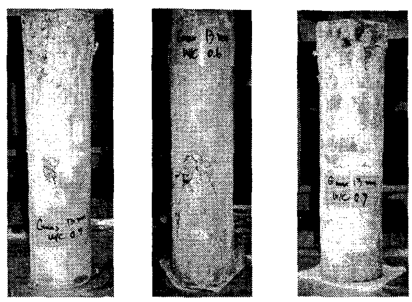

W/C=0.50 *W/C=0.60* *W/C=0.70*

(b) G_{max} = 13 mm

Fig.6 Cracking patterns of tested specimens (experiment Part II) significant difference in cracking patterns when specimens have different concrete properties.

It is of interest to notice that the slope of each local stress-strain curve shown in Fig.2 (b) (refer to also APPENDIX A) is different. A possible reason for this is that, when loading was applied, the volume of the specimen began to decrease as the length shortened, and this was followed later by lateral expansion. However, due to the residual frictional restraint at each end of the specimen, despite the attempt to eliminate it, and because of the inhomogeneity of concrete itself, expansion at the top and bottom was different. In the case of PS10-40 (Fig.3 (c)), the bottom expansion seems to be larger than that at the top, while more shortening is seen at the top, i.e. it has not yet expanded. Therefore, the ascending curves of local gages positioned near the top of the specimen show significant changes in longitudinal strain, whereas nearer the bottom, and especially at gage 10, only a slight change takes place, as can be seen from Fig.2 (b). On the other hand, after the peak load, the lower portion, where expansion is greater than at the top, fails in the final state; in other words, failure is localized at the bottom. This also confirms the concept that most of the applied energy is absorbed within the localized failure zone. This can be seen from area under the local strain curves, i.e. the higher A_{inti} at gages positioned on the lower half as compared with the upper ones.

In conclusion, the test results show in all cases for specimens whose length is greater than L_p, the final failure pattern is a combination of a few long penetrating cracks and a zone containing lots of small splitting cracks. The penetrating cracks are, in general, in the diagonal shear band, but in this study the frictional restraint at both ends of the specimens was eliminated in the tests, so the deviation of the crack inclination from the vertical is relatively small. The zone containing the splitting cracks, which indicate volumetric failure, contributes to the failure of most specimens; as a result, in this research, the determination of L_p is based on the length of this zone. Accordingly, G_{Fc}, which is defined as the energy required to cause compressive failure of a unit volume of the specimen, can then be calculated based on the externally applied energy and the localized failure volume, i.e. the zone containing splitting cracks, as described in detail in the Sections 6 and 7.

6. LOCALIZED COMPRESSIVE FRACTURE LENGTH, L_p

6.1 Effects of geometrical parameters

The effects of each geometrical parameter are discussed below for cases except H/D=1.

a) Height-depth ratio

By including also the results from experiment Part II, Fig.7 shows that the variation of H/D of a specimen causes no significant change to L_p. An average L_p value of almost 120 mm was obtained for both H/D=2 and 4 cases. In other words, a change in height of a specimen of a particular cross-section has no significant effect on L_p. The results for PR20-80 are excluded from this consideration because at the final stage a long penetrating crack from top to bottom was observed, indicating that the specimen failed with a different failure mode.

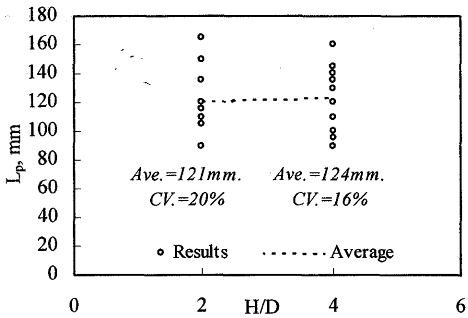

Fig.7 Variation of L_p with H/D ratio

b) Size and shape of specimen

From Fig.8, it can be observed that, for specimens having the same type of cross-section, an increase in cross-sectional area leads to a slight decrease in L_p while the square and rectangular cross-section specimens show slightly higher values of L_p compared with cylindrical specimens.

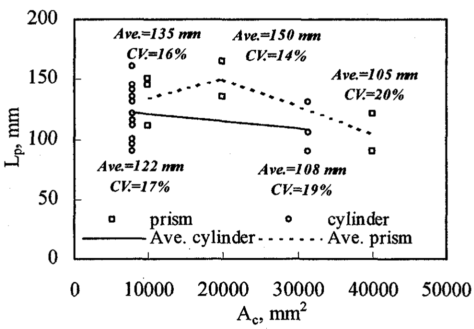

Fig.8 Variation of L_p with the cross-section and shape of specimens

6.2 Effects of concrete properties

The relationship between the experimentally obtained localized compressive fracture length and the cylindrical compressive strength is plotted in Fig.9.

It can be seen that, regardless of f_c' and G_{max}, L_p is almost constant with an average value of 120 mm and a coefficient of variation of 11%. That means, in comparison with geometrical parameters, G_{max} and W/C have little effect on the localized compressive fracture length of a specimen.

6.3 Formulation of L_p

As noted above, the height and shape of a specimen and also properties of the concrete used to cast it have virtually no effect on L_p, whereas L_p evidently dependent on the cross-sectional area. Therefore, the relation between L_p and the cross-section of a specimen given in terms of D^*, the equivalent cross-section width or the square root of cross-sectional area, A_c, is considered. The plot of concrete cross-sectional area against L_p/D^* in Fig.10 (a) shows that, within the range of the tests, an almost constant value of L_p/D^* is obtained when D^* is less than 100 mm (A_c<10,000 mm^2). An increase in A_c above this leads to a decrease in L_p/D^* in which the rate of decrease gradually falls. In order to simplify the relationship, a constant value of L_p/D^* for D^* larger than 180 mm (A_c>32,400 mm^2) is assumed.

Finally, the following simplified relationship can be proposed:

$$
\begin{aligned}
L_p/D^* &= 1.36 && ;\ D^*<100 \\
&= -3.53\times 10^{-5} D^{*2} + 1.71 && ;\ 100 \le D^* \le 180 \qquad (3) \\
&= 0.57 && ;\ D^*>180 \qquad \text{(mm)}
\end{aligned}
$$

where, $D^* = \sqrt{A_C}$, mm

, as depicted in Fig.10 (b).

The effects of various concrete specimen parameters on L_p, which were obtained from direct measurements, were also studied by Nakamura and Higai[4]. They performed uniaxial compressive tests on concrete cylinders measuring ϕ 100 and ϕ 150 mm with a range of H/D ratios, and found that H/D has little effect on L_p, reflecting the results obtained in this study. However, their results further showed that the cross-sectional area of a specimen has no effect on L_p, while L_p is rather affected by f_c' and the size and grading of the aggregates. This may be because of the narrower range of cross-sectional area in their test. In addition, L_p was not quantitatively evaluated, which differs from the process presented here. In contrast, according to experimental research done by Rokugo and Koyanagi[9], L_p tended to be constant for concrete specimens with the same cross-sectional area.

7. COMPRESSIVE FRACTURE ENERGY, G_{Fc}

As mentioned above, one-directional repeated loading in the stress descending range was carried out so as to capture the stress-strain curve within the post-peak region. However, for specimens with comparatively large cross-section, a sudden drop in load at the peak point was, for some reasons, unavoidable. Furthermore, G_{Fc} is substantially dependent on the area under the load-overall deformation curve or the shape of the curve itself, especially in the descending range. Therefore, in order to obtain the most reliable results, the results of the C20 and PS20 series were not included in the consideration of G_{Fc}. Thus, Fig.11 was plotted omitting these.

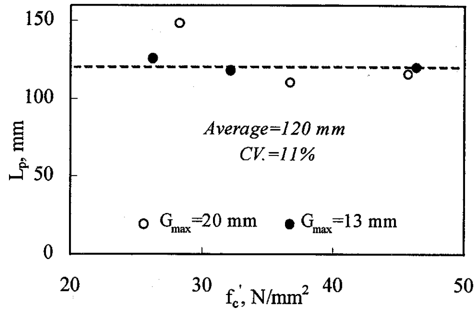

Fig.9 Relationship between L_p and concrete cylinder compressive strength

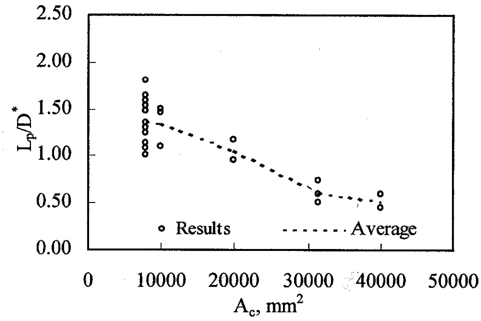

(a) Experimental results

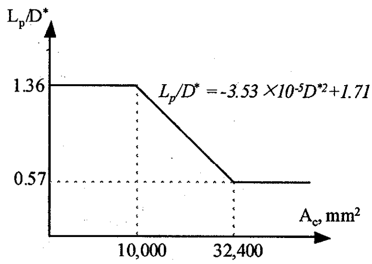

(b) Proposed formulation

Fig.10 Relation of L_p and equivalent width of the specimen

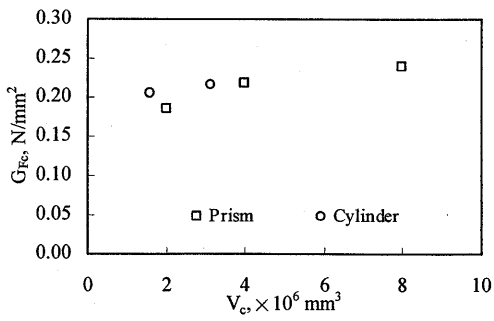

(a) G_{Fc} and V_c

Fig.11 Relationship between G_{Fc} and parameters in the tests

7.1 Effects of geometrical parameters

Figure 11 (a) shows the relationship between the total specimen volume, V_c, and the average value of G_{Fc} for cylindrical and prism specimens. In order to isolate the effects of the geometrical parameters, the results of Part II were not included. It can be seen that there was almost no change in G_{Fc} with changes in the geometry of specimens.

7.2 Effects of concrete properties

Figure 11 (b) shows that the value of G_{Fc} is, in some way, dependent on the cylindrical compressive strength. It is found that when G_{Fc} is divided by $f_c'^{1/4}$, an almost constant average value of 0.86×10^{-1} with a coefficient of variation of 18% is obtained, as shown in Fig.11 (c).
On the other hand, from Fig.12 it can be seen that the maximum size of coarse aggregate has little effect on the magnitude of G_{Fc}.

7.3 Formulation of G_{Fc}

From Fig.11(c), the following simplified relationship can be obtained for when localization in compression occurs:

$$G_{Fc} = 0.86\times10^{-1} f_c'^{1/4} \qquad (4)$$

where, the units of G_{Fc} and f_c' are N/mm^2.

This formulation is consistent with previous research work[4] in that the fracture energy in compression depends on concrete compressive strength regardless of the size and shape of the concrete specimen. Though the coefficient and the power of f_c' in the formulation are different because of the difference in the calculation of G_{Fc} but it can be conceived that the relation between G_{Fc} and f_c' is nonlinear.

However, the actual cracking pattern of a concrete specimen comprises a zone containing lots of small cracks and a small number of penetrating long cracks. The calculation of G_{Fc} here is based on only the small cracking zone, which is simulated by the localized fracture volume, while the long penetrating cracks and the unloading portion that absorb some part of the external applied energy are not taken into consideration. Note that the results for PR20-80 were also not included here because the final failure pattern of the specimen, which consisted of a long and wide open splitting crack from top to bottom and only few small tensile splitting cracks, is considerably different from the other specimens.

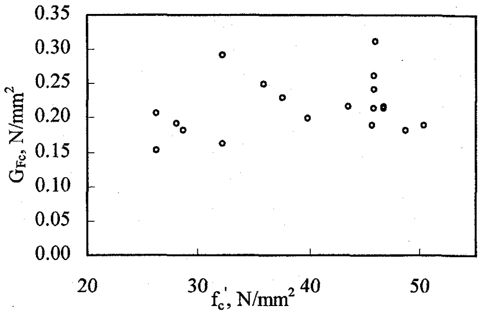

(b) G_{Fc} and f_c'

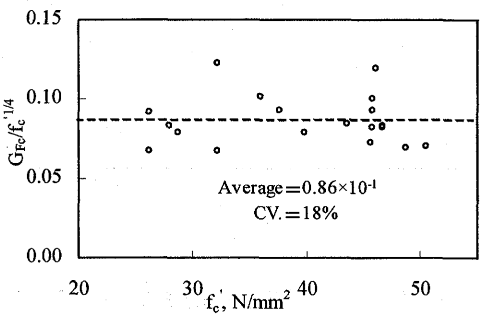

(c) G_{Fc} and $f_c'^{1/4}$

Fig.11 Relationship between G_{Fc} and parameters in the tests (continued)

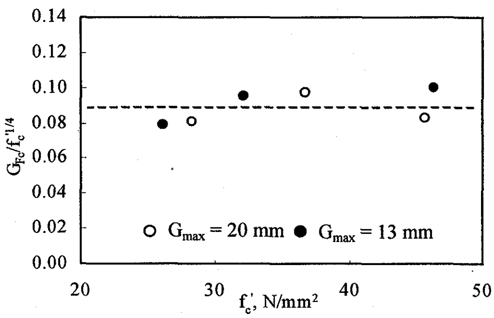

Fig.12 Relationship between G_{Fc} and f_c'

8. CONCLUDING REMARKS

Through the technique of measuring the local strain within a concrete specimen along its axis, localization of the failure in uniaxial compression is shown to occur when the specimen has an H/D ratio greater than or equal to 2. The localized compressive fracture length can be evaluated from the relative amount of energy absorbed by each portion of the specimen. The method presented here offers a new quantitative means of determining the value of L_p, and the results obtained are found to agree with observations made during the testing procedure.

The localized compressive fracture length is found to be dependent solely on the specimen cross-section, whereas the specimen height, H/D ratio, and cross-sectional shape are found to have less effect on L_p. The cylindrical compressive strength and the maximum size of aggregate of the specimen concrete are found to have virtually no effect on localized compressive fracture length. A relation between L_p and the equivalent section width is proposed.

Subsequently, the fracture energy in compression is calculated by dividing the area under the load-overall deformation curve by the fracture volume. This concept is different from previous research work which, in most cases, did not taken into account the effect of the localized failure zone. The test results indicate that G_{Fc} varies with changes in concrete cylindrical compressive strength, while changes in geometry of the specimen and the maximum size of aggregate used in casting have less effect on G_{Fc}. A relation between G_{Fc} and f_c' is proposed.

The obtained G_{Fc} values do not take into consideration the contribution from penetrating cracks and the unloading portion; further studies are needed in order to gain a better understanding of localization behavior in compression.

APPENDIX A TEST RESULTS FOR PS10-40

The applied stress-local strain curves for PS10-40 are depicted in detail in Fig.A1. Each curve represents the path obtained from one-directional repeated loading in the stress descending range, and the envelope obtained by connecting the peak points of the repeated curve is also shown.

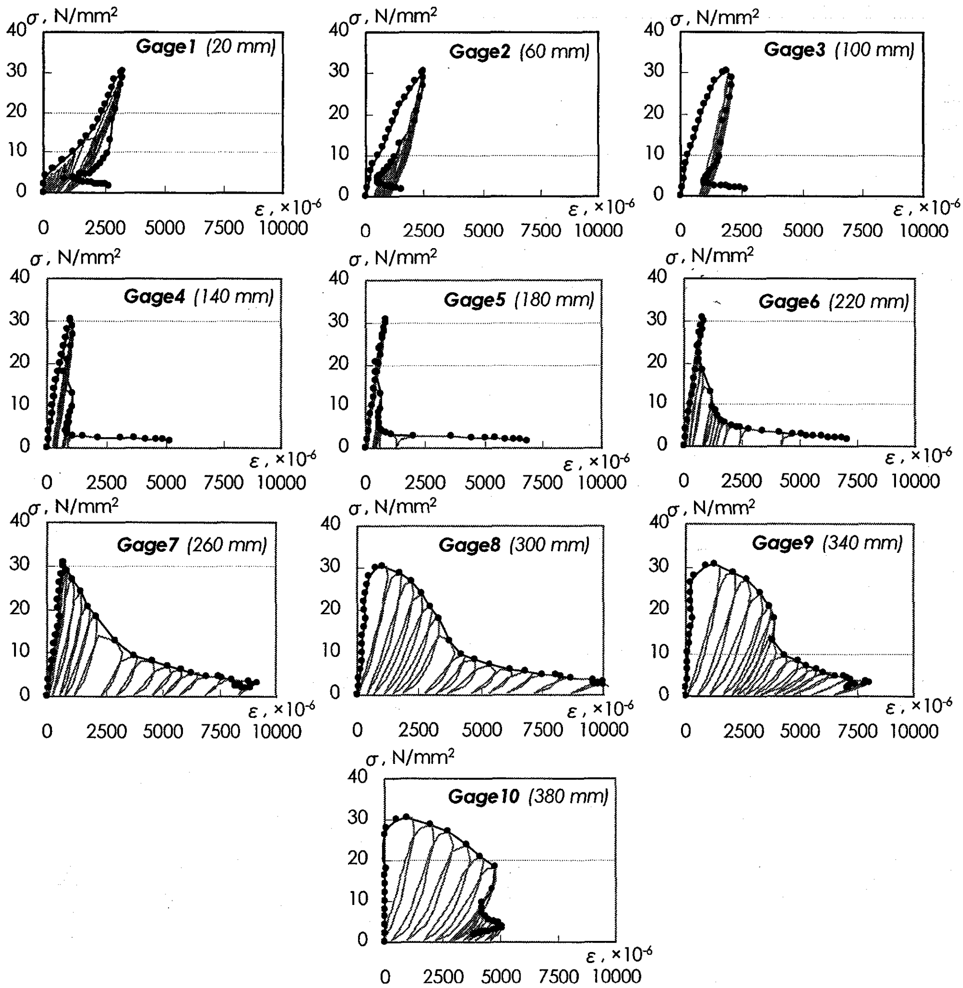

Fig.A1 Results for PS10-40 (Gage 1-10)

APPENDIX B USE OF ACRYLIC BAR

The effectiveness of local strain measurements using a deformed acrylic bar was investigated by comparing the deformation measured externally by deflection gages with the accumulated calculated deformation from the local strain gages throughout the whole length of a specimen. It was found that the two sets of results agreed with each other well until the peak load was reached. After the peak load, the calculated deformation from local strain gages was slightly smaller than that indicated by the deflection gages, as shown in Fig.B1. This deviation occurs because, once the maximum resistance is reached, cracking takes place in the specimen; at this point the deflection gages continue measuring the overall-averaged deformation, whereas the calculated deformation from local strain gages is, in some way, evaluated based on the magnitude of the strain measured at the location of the strain gages and is the average figure for the interval between gages. However, the difference is negligibly small, so the use of a deformed acrylic bar with attached strain gages to measure the internal local strain is considered reliable.

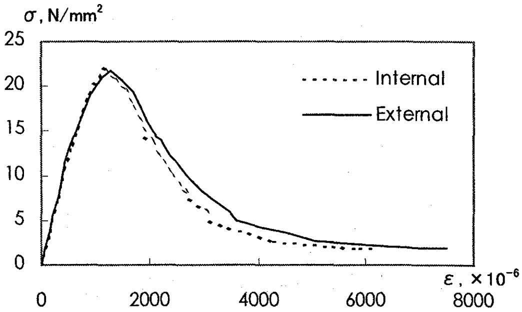

Fig.B1 Comparison between the externally (deflection gages) and internally (local strain gages) measured strain (ϕ 100×400, G_{max}=13 mm, W/C=70%)

References

1) Bažant, Z. P. and Oh, B. H.: Crack Band Theory for Fracture of Concrete, *Materials and Structures*, Vol. 16, No.93, pp. 155-177, 1983.
2) Santiago, S. D. and Hilsdorf, H. K.: Fracture Mechanisms of Concrete under Compressive Loads, *Cement and Concrete Research*, Vol. 3, pp. 363-388, 1973.
3) Sangha, C.M. and Dhir, R.K.: Strength and Complete Stress-strain Relationships for Concrete Tested in Uniaxial Compression under Different Test Conditions, *RILEM, Materiaux et Constructions*, Vol. 5, pp. 361-370, 1972.
4) Nakamura, H. and Higai, T.: Compressive Fracture Energy and Fracture Zone Length of Concrete, *JCI-C51E Seminar on Post-Peak Behavior of RC Structures Subjected to Seismic Loads*, Vol. 2, pp. 259-272, Oct. 1999.
5) Markeset, G.: Failure of Concrete under Compressive Strain Gradients, *Dr.Ing thesis 1993:110,* Norwegian Institute of Technology, Trondheim, 1993.
6) Hillerborg, A.: Fracture Mechanics Concepts Applied to Moment Capacity and Rotational Capacity of Reinforced Concrete Beams, *Engineering Fracture Mechanics*, Vol. 35, No. 1/2/3, pp. 223-240, 1990.
7) Markeset, G. and Hillerborg, A.: Softening of Concrete in Compression – Localization and Size Effects, *Cement and Concrete Research*, Vol. 25, No. 4, pp. 702-708, 1995.
8) Newman, K. and Lachance, L.: The Testing of Brittle Materials under Uniform Uniaxial Compression Stress, *Proc. ASTM*, Vol. 64, pp. 1044-1067, 1964.
9) Rokugo, K. and Koyanagi, W.: Role of Compressive Fracture Energy of Concrete on the Failure Behavior of Reinforced Concrete Beams, in *Applications of Fracture Mechanics to Reinforced Concrete (ed. A. Carpinteri),* Elsevier Applied Science, pp. 437-464, 1992.
10) Kotsovos, M.D.: Effect of Testing Techniques on the Post-Ultimate Behaviour of Concrete in Compression, , *RILEM Materials and Structures*, Vol. 16, No. 91, pp. 3-12, 1983.